# Experimental study of the effect of surface groove micro-texturing on lubrication characteristics

*Huichao Gao*[1,2], *Xinyuan Chen*[1,2] ✉

[1]*Key Laboratory of Metallurgical Equipment and Control Technology, Wuhan University of Science and Technology, Ministry of Education, Wuhan, Hubei 430081, People's Republic of China*
[2]*Hubei Key Laboratory of Mechanical Transmission and Manufacturing Engineering, Wuhan University of Science and Technology, Wuhan, Hubei 430081, People's Republic of China*
✉ *E-mail: chenxinyuan@wust.edu.cn*

Published in Micro & Nano Letters; Received on 13th June 2019; Revised on 7th February 2020; Accepted on 6th March 2020

This study investigated the effect of surface groove micro-texturing on hydrodynamic lubrication characteristics. All textured samples were processed by laser; non-textured reference samples were also created for comparison. Four types of surface groove patterns with different groove angles and groove depths were utilised. Different rotational speeds and gaps were used in the experiment to explain the relationship between the load-carrying capacity and the groove texture parameters under different conditions. The results suggested that the load-carrying capacity was greatly influenced by the operational conditions and that the samples with surface groove textures generated a larger hydrodynamic lift force than the non-textured samples.

**1. Introduction:** The piston pump is a commonly used power component in hydraulic systems. Its performance is directly related to the working efficiency of the system. A clearance fit is applied between the piston and the cylinder bore, and a suitable gap size can both seal and prevent the piston from becoming stuck. In the initial stage of the piston pump operation, the piston is subjected to a large viscous force. Fig. 1 provides a schematic diagram of the piston pump. To improve the lubrication performance at the clearance fit, the piston and cylinder bore maintain a low friction and wear rate, and surface texture is introduced. The use of surface textures, such as micro-dimples or grooves, is a well-known approach to improve the lubrication status of mating pairs. In 1966, Hamilton studied the rotary-shaft face seal and found that micro-irregular cavities can produce a load capacity under certain conditions [1]. After this discovery, many scholars began to pay attention to this surface texturing technology.

One of the most dominant effects provided by surface textures is the creation of additional load capacity in the lubrication region. Under a starved lubrication condition, surface textures act as oil reservoirs, providing lubricant to the contact area or entrapped wear debris [2, 3]. The research on surface textures can be divided into theoretical and experimental approaches. With the theoretical approach, numerous studies have utilised the Reynolds equation or the Navier–Stokes equations to analyse the mechanism behind textured surfaces [4–7]. For example, Bai *et al*. [8] numerically investigated partial texturing with elliptical dimples, and the results showed that the orientation of dimples can greatly enhance the hydrodynamic effect. Yu *et al*. [9] established theoretical models for three shapes (circular, triangular and elliptical), and the results showed that for diverse shapes and orientations, the load capacity is different. By establishing a model of the surface groove texture, Mezghani *et al*. [10] and Biboulet *et al*. [11] found that the surface texture can reduce friction and change the load-carrying capacity under some conditions.

Theoretical research can reveal the mechanism of action for surface texture, but experiments are the most direct way to test the performance of the surface texture. Different topographic parameters [12] and arrangements [13] provide different performances. For example, Vilhena *et al*. [14] conducted tribological experiments on samples with different texture densities, and the results showed that with boundary lubrication, the presence of texture increases friction. Costa experimentally compared the performances of several different textured shapes (circular depressions, grooves and chevrons) and found that chevrons are the most significant in increasing film thickness [15]. Yu *et al*. [16] and Chen *et al*. [17] studied the hydrodynamic performance of triangular dimples, and the surface texturing was effective in reducing friction. Moreover, the lubrication and friction reduction properties of the surface texture are related to the lubrication conditions [18, 19].

Most of the aforementioned articles were carried out under different contact conditions (points, lines, or faces); however, few studies have focused on the effects of gaps on lubrication performance and the load-carrying capacity. At the same time, many researchers are concerned with the contrast between several different shapes of texture. There are few experimental studies on the different parameters and operational conditions of the groove texture. In this Letter, samples with two types of depth and four different angles were used in the experiment, and the experimental variables were the rotational speed and the gap of the plates. The load-carrying capacity of the different textured samples under the same experimental conditions was determined, and the results suggested that the grooved surface texture can improve lubrication performance and that the load-carrying capacity is greatly influenced by the operational conditions.

## 2. Experimental details

2.1. Experimental apparatus: The experiments were carried out on a rheometer (AR2000ex) under full lubrication conditions, and Table 1 presents the technical parameters of the instrument. The probe had a 40 mm diameter. During testing, the sample was fixed to the bottom of the reservoir with screws. A schematic diagram of the experimental instrument is shown in Fig. 2.

2.2. Samples: There are several ways to implement the surface micro-texture processing, for example, reactive ion etching [20], surface shot peening [21], femtosecond laser processing [22] and other surface texture processing techniques. The processing method selected in this Letter was femtosecond laser processing. Femtosecond lasers have become increasingly prevalent in precision manufacturing because they are high-quality tools for micro-processing various materials, such as metals [23, 24], semiconductors [25] and dielectrics.




doi: 10.1049/mnl.2019.0361

**Table 1** Technical parameters of AR2000ex

| | |
|---|---|
| dynamic oscillating minimum torque | 0.03 μN·m |
| steady state minimum torque | 0.05 μN·m |
| maximum torque | 200 mN·m |
| torque resolution | 1 μN·m |
| angular velocity range | $1\times10^{-8}$–300 rad/s |
| frequency range | $7.5\times10^{-7}$–628 rad/s |
| axial force range | 0.005–50 N |
| speed switching interval | 25 ms |
| stress switching interval | 1 ms |

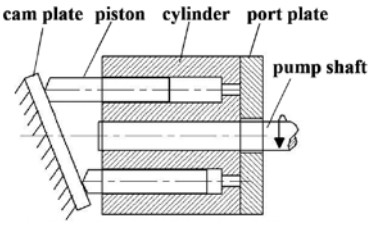


**Fig. 1** *Assembly of a piston pump*

In this work, NO. 45 steel (C45) was selected for the test sample material. Before laser surface texturing, the surface of each sample was precision ground to a surface roughness of 0.8 μm. After processing, the samples were ultrasonically cleaned with ethanol to remove any grinding debris. Fig. 3 includes a schematic diagram of laser surface texturing by the Femto YL$^{TM}$-50 laser process system.

The bottom plate of each sample was a disc with a diameter of 60 mm, and a 20 mm × 20 mm square in the middle of the disc served as the area for processing the surface groove texture.

To compare and analyse the influences of angle and depth on the lubrication behaviour, four different angles and two different depths were utilised. Sample A was a non-textured plane that was designed for comparison. The parameters of the other textured samples are shown in Table 2. Fig. 4 shows a schematic diagram of surface groove texture parameters.

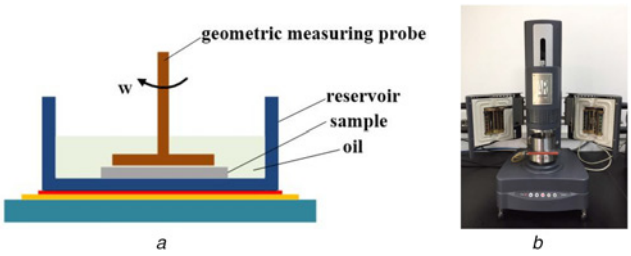


**Fig. 2** *Schematic diagram of the instrument*
*a* Sketched diagram of the instrument
*b* Photo of the instrument

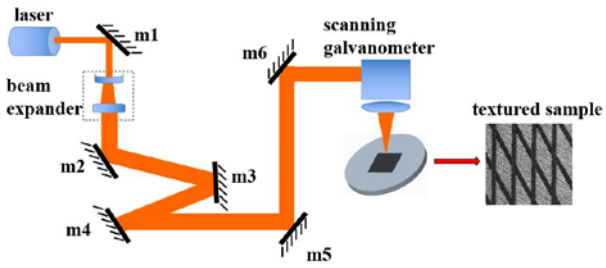


**Fig. 3** *Laser surface texturing by the Femto YL$^{TM}$-50 laser process system*

**Table 2** Parameters of surface groove textures

| Sample | *a*, μm | *c*, μm | *d*, μm | Θ, deg |
|---|---|---|---|---|
| E1 | 900 | 180 | 20 | 30 |
| E2 | 900 | 180 | 20 | 45 |
| E3 | 900 | 180 | 20 | 60 |
| E4 | 900 | 180 | 20 | 90 |
| E5 | 900 | 180 | 40 | 30 |
| E6 | 900 | 180 | 40 | 45 |
| E7 | 900 | 180 | 40 | 60 |
| E8 | 900 | 180 | 40 | 90 |

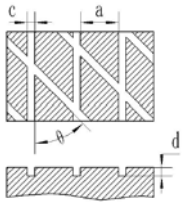


**Fig. 4** *Schematic diagram of the surface groove texture parameters*

2.3. Experimental conditions: The axial force between the sample and the geometric measuring probe was zeroed before the start of the experiment. The axial force between the sample and the geometric measuring probe was determined in the experiment, with the load-carrying capacity being the measured axial force. In the experiment, the gap between the probe and the sample was maintained at a fixed value, which was convenient for measuring the load capacity of the film. Herein, the gap was set to 10 and 20 μm. L-HM-46 oil was the lubricating oil employed in the experiments. Table 3 shows the basic properties of the oil. All tests were conducted at a room temperature of 20°C and relative humidity of 40%.

2.4. Data processing: In the rheometer tests, the rotational speed was determined by the peak hold mode, and the rotational speed of the geometric measuring probe was set to 20, 40, 60, 80, 100, and 120 rad/s. The test duration was 300 s at each peak speed. The axial force was measured at intervals of 5 s during each test, i.e. the axial force was measured 60 times per test.

Fig. 5 shows the results of one test (sample E1 with a gap of 10 μm). As seen from the figure, the load-carrying capacity fluctuated slightly during the whole experiment. Under all speed conditions, each curve tended to stabilise after exhibiting a small change, which indicates that the load-carrying capacity stabilised.

Therefore, we did not consider the measured values from the unstable phase (from the beginning to 50 s). To ensure the reliability of the data, all tests were repeated at least 3 times.

## 3. Results and discussion

3.1. Effects of the rotational speed and gap: Fig. 6 compares sample A and sample E2 to illustrate the effects of different rotational speeds and gaps on the load-carrying capacity. The figure indicates that the load-carrying capacity increases with the rotational speed,

**Table 3** Basic properties of the oil

| Parameter | Value |
|---|---|
| density at 20°C, kg/m$^3$ | 870 |
| flash point, °C | ≥175 |
| kinematic viscosity at 40°C, mm$^2$/s | 46 |
| kinematic viscosity at 20°C, mm$^2$/s | 150 |

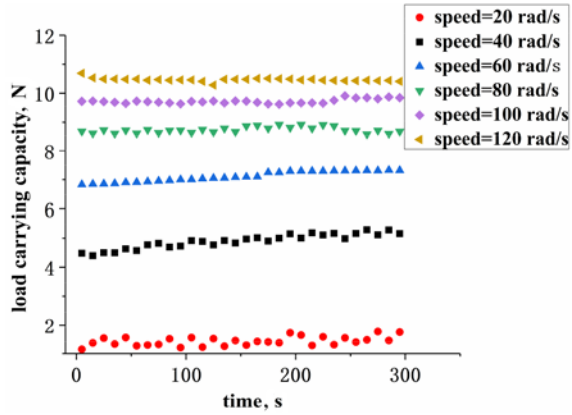


**Fig. 5** *Results of one test (sample E1 with a gap of 10 μm)*

whereas the load-carrying capacity decreases when the gap increases; these trends suggest that the load-carrying capacity is influenced by the sliding speed and gap to a certain extent.

Sample E2 performs better than sample A under any condition. For both 10 and 20 μm gaps, sample E2 exhibits a higher load-carrying capacity than that of sample A throughout the entire experiment, and the growth rate of the load-carrying capacity of sample E2 is also larger than that of sample A. One possible reason for this phenomenon is that the surface groove texturing decreases the contact area, thereby reducing adhesion and generating hydrodynamic pressure to produce additional lift [26, 27]. Because of the generation of an additional hydrodynamic lift, the lubrication performance of sample E2 is superior to that of sample A for different gaps. The error bar of the sample E2 at a gap of 20 μm is significantly larger than the other groups, the error bars explains the fluctuations in the data, and this shows that the texture performs better with a gap of 10 μm. The figure also shows that the difference in the load-carrying capacity between the samples for different gaps is small at the beginning of the experiment, gradually increases during the experiment, and finally stabilises.

Due to the rotational motion, regardless of a textured or a smooth surface, the velocity of the fluid on the entire surface exhibits a gradient distribution in the radial direction. This behaviour is due to the flow rate of the oil in the groove of the texture being significantly lower than the flow rate of the oil on the surface. Therefore, a flow different from the flow pattern of the surface is generated, and these two irregular flows explain to some extent the effects of hydrodynamic lubrication. The phenomenon of hydrodynamic lubrication on the surface of the groove texture is mainly due to the movement of the flow velocity in two different directions. Irregular flow serves as the driving force behind hydrodynamic

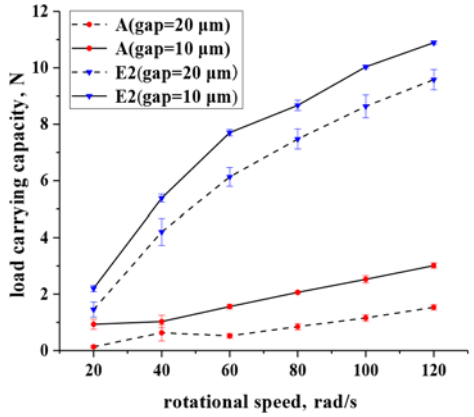


**Fig. 6** *Performance of samples for different rotational speeds and gap sizes*

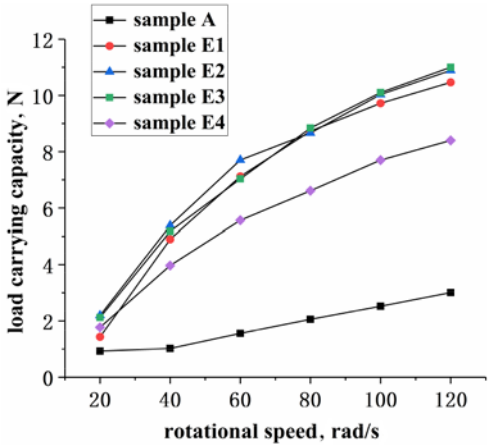


**Fig. 7** *Performance of samples with different groove angles for a 10 μm gap*

lubrication. In parallel, the change in the gap corresponds to a change in the thickness of the oil film, and a decrease in the thickness of the oil film can significantly increase the load-carrying capacity.

3.2. Effect of the groove angle: Fig. 7 shows the variation in the load-carrying capacity with respect to the rotational speed for the samples with different groove angles. In this figure, samples E1, E2, E3 and E4 have the same parameters except for the groove angle; note that the groove depth for these samples is 20 μm. As revealed by the figure, no matter how the rotational speed changes, the load-carrying capacity is improved due to the surface texture. The textured surface with different geometric angles also expresses varying degrees of enhancement in the lubrication performance. At a rotational speed of 20 rad/s, the load-carrying capacity of all samples is small, the performance of sample E1 appears to be slightly worse than that of sample E4. However, when the rotational speed is increased, the growth curves for samples E1, E2 and E3 are nearly coincident. Overall, samples E1, E2 and E3 perform better than sample E4, and all samples with surface groove textures perform better than the non-textured sample A.

As evidenced by the curve data, the textured sample provides a load-carrying capacity 2–3 times that of sample A. The diamond-shaped unit structure achieves the effect of reducing the fluid resistance. The groove structure reduces the effective friction surface and frictional strength of the surface and fluid, thereby reducing the shear pressure. The data in the figure indicate that the oil reduction effect is greater when the angle is smaller, e.g. the drag reduction effect at 90° is not as good as that at small angles. The simulation analysis by Mezghani *et al.* [10] showed that angles of 40°–55° and 115°–130° provide the minimum friction coefficient, while Biboulet *et al.* [11] used a curve-fitting approach and determined that angles between 25° and 75° produce the minimum friction coefficient. These results suggest that the lubrication is optimal in this angle range, which is similar to the experimental result of this Letter.

3.3. Effect of depth: The two plots in Fig. 8 provide a comparison of the load-carrying capacities of all textured samples at different rotational speeds. In the experiment, the gap was set to 10 μm. The figures show the average values of the load-carrying capacity at different rotational speeds. As indicated by the two plots, the load-carrying capacity increases with the rotational speed. The load-carrying capacity curves for samples with a groove depth of 20 μm are always above the curves for samples with a groove depth of 40 μm; this result means that the performance for a texture depth of 20 μm is always better than that for a depth of 40 μm.

The fluid flow on the surface with the mesh texture unit and the groove form a dynamic-pressure lubrication phenomenon




doi: 10.1049/mnl.2019.0361

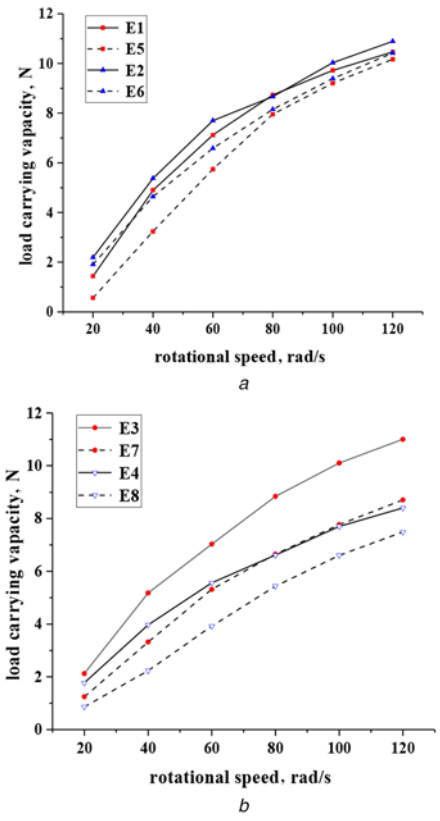


**Fig. 8** *Performance of samples with different depths for a 10 μm gap*
*a* Comparison of samples E1, E5, E2 and E6
*b* Comparison of samples E3, E7, E4 and E8

that is complicated. A pressure gradient is a key to affecting the lift generated by the fluid. For the formation of the lifting force on the upper surface, a main surface-related factor is a change in the surface gap. Here, a wedge shape was used to change the constant gap with the parallel surface to achieve the effect of hydrodynamic lubrication. The surface height difference between the diamond-shaped unit and the groove structure creates a varying surface gap, which contributes to the generation of dynamic pressure.

The flow of oil over the textured surface presents two states between the textured grooves and the gap between the two surfaces. The oil flow path between the two surfaces is in the direction of rotation, and the groove of the textured surface impedes the oil to a certain extent. Therefore, these two irregular flows partially explain the behaviour of hydrodynamic lubrication. The experimental results indicate that the effect produced by a depth of 20 μm is better than the effect achieved with a depth of 40 μm.

**4. Conclusion:** In this Letter, the lubrication properties of samples surface textured with grooves under full lubrication conditions were studied experimentally. All samples in the experiment were discs and partially textured. The load-carrying capacity of the film under different operational conditions was measured by controlling the rotational speed and the gap between the samples as well as the geometric measuring probe. The experimental results reveal that the textured samples exhibit a performance that is better than that of the non-textured samples under the same operational conditions. Significant observations include the following:

(i) When the gap is the same, the load-carrying capacity increases with the rotational speed. When the rotational speed is the same, the loading carrying capacity at a gap of 10 μm is better than that at 20 μm. Regardless of the gap and speed, the textured samples perform better than the non-textured samples.

(ii) The textured samples exhibit lubrication properties superior to those of the non-textured sample under the same experimental conditions. Samples with groove angles of 30°, 45° and 60° present an evident advantage over samples with other groove angles.

(iii) As the groove depth of the sample increases, the load-carrying capacity decreases, whereas the load-carrying capacities of the samples with 30° and 45° texture angles maintain highly stable values as the groove depth increases.

**5. Acknowledgments:** This work was supported by the National Natural Science Foundation of China under (grant nos. 51875417 and 51975425).

## 6 References

[1] Hamilton D.B., Walowit J.A., Allen C.M.: 'A theory of lubrication by micro-irregularities', *Trans. ASME J. Basic Eng.*, 1966, **88**, pp. 177–185
[2] Xiong D.S., Qin Y.K., Li J.L., *ET AL.*: 'Tribological properties of PTFE/laser surface textured stainless steel under starved oil lubrication', *Tribol. Int.*, 2015, **82**, pp. 305–310
[3] Varenberg M., Halperin G., Etsion I.: 'Different aspects of the role of wear debris in fretting wear', *Wear*, 2002, **252**, pp. 902–910
[4] Sahlin F., Glavatskih S., Almqvist T., *ET AL.*: 'Two-dimensional CFD-analysis of micro-patterned surfaces in hydrodynamic lubrication', *J. Tribol.-T ASME*, 2005, **127**, pp. 96–102
[5] Feldman Y., Kligerman Y., Etsion I., *ET AL.*: 'The validity of the Reynolds equation in modeling hydrostatic effects in gas lubricated textured parallel surfaces', *J. Tribol.*, 2005, **128**, pp. 345–350
[6] Qiu M., Bailey B.N., Stoll R., *ET AL.*: 'The accuracy of the compressible Reynolds equation for predicting the local pressure in gas-lubricated textured parallel slider bearings', *Tribol. Int.*, 2014, **72**, pp. 83–89
[7] Marian V.G., Predescu A., Pascovici M.D.: 'Theoretical analysis of an infinitely wide rigid cylinder rotating over a grooved surface in hydrodynamic conditions', *Proc. Inst. Mech. Eng. J, J. Eng. Tribol.*, 2009, **224**, pp. 757–763
[8] Bai S., Peng X., Li Y., *ET AL.*: 'A hydrodynamic laser surface textured gas mechanical face seal', *Tribol. Lett.*, 2010, **38**, pp. 187–194
[9] Yu H., Wang X., Zhou F.: 'Geometric shape effects of surface texture on the generation of hydrodynamic pressure between conformal contacting surfaces', *Tribol. Lett.*, 2010, **37**, pp. 123–130
[10] Mezghani S., Demirci I., Zahouani H., *ET AL.*: 'The effect of groove texture patterns on piston-ring pack friction', *Precis Eng.*, 2012, **36**, pp. 210–217
[11] Biboulet N., Bouassida H., Lubrecht A.A.: 'Cross hatched texture influence on the load carrying capacity of oil control rings', *Tribol. Int.*, 2015, **82**, pp. 12–19
[12] Wang X., Kato K., Adachi K., *ET AL.*: 'Loads carrying capacity map for the surface texture design of SiC thrust bearing sliding in water', *Tribol. Int.*, 2003, **36**, pp. 189–197
[13] Chen J., Zeng L., Wu Z., *ET AL.*: 'Experimental investigation of disc partial surface texture on the generation of hydrodynamic lubricating performance under conformal contact condition', *AIP. Adv.*, 2018, **8**, pp. 125205-1–125205-9
[14] Vilhena L.M., Ramalho A., Cavaleiro A.: 'Grooved surface texturing by electrical discharge machining (EDM) under different lubrication regimes', *Lubr. Sci.*, 2017, **29**, pp. 493–501
[15] Costa H.L., Hutchings I.M.: 'Hydrodynamic lubrication of textured steel surfaces under reciprocating sliding conditions', *Tribol. Int.*, 2007, **40**, pp. 1227–1238
[16] Yu H., Huang W., Wang X.: 'Dimple patterns design for different circumstances', *Lubr. Sci.*, 2011, **25**, pp. 67–78
[17] Chen P., Xiang X., Shao T., *ET AL.*: 'Effect of triangular texture on the tribological performance of die steel with TiN coatings under lubricated sliding condition', *Appl. Surf. Sci.*, 2016, **389**, pp. 361–368
[18] Braun D., Greiner C., Schneider J., *ET AL.*: 'Efficiency of laser texturing in the reduction of friction under mixed lubrication', *Tribol. Int.*, 2014, **77**, pp. 142–147
[19] Wos S., Koszela W., Pawlus P., *ET AL.*: 'Effects of surface texturing and kind of lubricant on the coefficient of friction at ambient and elevated temperatures', *Tribol. Int.*, 2018, **117**, pp. 174–179

[20] Erdemir A.: 'Review of engineered tribological interfaces for improved boundary lubrication', *Tribol. Int.*, 2005, **38**, pp. 249–256
[21] Sudeep U., Tandon N., Pandey R.K.: 'Performance of lubricated rolling/sliding concentrated contacts with surface textures: a review', *J. Tribol.-T ASME*, 2015, **137**, pp. 031501-1–031501-11
[22] Wang Z., Li Y.B., Bai F.: 'Angle-dependent lubricated tribological properties of stainless steel by femtosecond laser surface texturing', *Opt. Laser Technol.*, 2016, **81**, pp. 60–66
[23] Momma C., Chichkov B.N., Nolte S., *ET AL.*: 'Short-pulse laser ablation of solid targets', *Opt. Commun.*, 1996, **129**, pp. 134–142
[24] Vonder Linde D., Sokolowski-Tinten K.: 'The physical mechanisms of short-pulse laser ablation', *Appl. Surf. Sci.*, 2000, **154–155**, pp. 1–10
[25] Sundaram S.K., Mazur E.: 'Inducing and probing non-thermal transitions in semiconductors using femtosecond laser pulses', *Nature Mater.*, 2002, **1**, pp. 217–224
[26] Tønder K.: 'Dynamics of rough slider bearings: effects of one-sided roughness/waviness', *Tribol. Int.*, 1996, **29**, pp. 117–122
[27] Tønder K.: 'Hydrodynamic effects of tailored inlet roughnesses: extended theory', *Tribol. Int.*, 2004, **37**, pp. 137–142




doi: 10.1049/mnl.2019.0361